

# Anderson orthogonality catastrophe in realistic quantum dots

Swarnali Bandopadhyay

*Department of Physics, Norwegian University of Science and Technology, N-7491, Trondheim, Norway\**

Martina Hentschel

*Max-Planck-Institut für Physik komplexer Systeme, Nöthnitzer Str. 38, 01187 Dresden, Germany*

(Dated: November 8, 2018)

We study Anderson orthogonality catastrophe (AOC) for an parabolic quantum dot (PQD), one of the experimentally realizable few-electron systems. The finite number of electrons in PQD causes AOC to be incomplete, with a broad distribution of many-body overlaps. This is a signature of mesoscopic fluctuations and is in agreement with earlier results obtained for chaotic quantum dots. Here, we focus on the effects of degeneracies in PQDs, realized through their inherent shell structures, on AOC. We find rich and interesting behaviours as a function of the strength and position of the perturbation, the system size, and the applied magnetic field. In particular, even for weak perturbations, we observe a pronounced AOC which is related to the degeneracy of energy levels. Most importantly, the power law decay of the many-body overlap as a function of increasing number of particles is modified in comparison to the metallic case due to rearrangements of energy levels in different shells.

PACS numbers: 73.21.-b, 05.45.Mt, 78.67.-n, 78.70.Dm

## I. INTRODUCTION

Anderson orthogonality catastrophe (AOC) is one of the simplest many-body effects in condensed matter physics. It was first described by Anderson [1] in 1967 and refers to the vanishing of the overlap between the unperturbed and perturbed many-body ground states as a power law in the number of particles in the system. This results from the non-adiabatic response of the system to a sudden perturbation. AOC contributes to a number of Fermi-edge singularities (FES), e.g., in the Kondo effect [2] or in the X-ray edge problem [3, 4, 5]. In the X-ray edge problem, the sudden and localised perturbation is realized through the X-ray excitation of a core electron that leaves behind a localised attracting (hole) potential. Here, other many-body responses may play a role, e.g., the so-called Mahan-Nozières-DeDominicis response or Mahan's exciton [3, 4] in FES of photoabsorption spectra. However, in the case of photo-emission experiments where the excited core electron leaves the sample, the physics is governed by AOC alone [6]. This will be our focus in this article.

AOC was originally introduced and discussed for bulk samples with a large number of particles (corresponding to the thermodynamic limit). The conduction electrons respond to the attractive core-hole potential by slightly lowering their single particle energy levels. Although the overlap between the single particle states before and after the photo-excitation remains very close to one, this is not true for the overlap between the corresponding many-body ground states. In AOC the many-body overlap between the unperturbed and perturbed ground states  $|\Delta|^2$

vanishes as a power law in the number of participating electrons  $M_{\text{eff}}$  as

$$|\Delta|^2 \propto M_{\text{eff}}^{-\phi^2},$$

with  $M_{\text{eff}} = \rho_c W_c$  where  $\rho_c$  is the density of states of the conduction band at the Fermi level and  $W_c$  is the width of the conduction band [5];  $\phi$  is the phase shift at the Fermi energy.

In recent years, the fabrication of high-quality samples with a finite number of electrons ranging from very few to, say, several thousands, has become possible. A hallmark example are the effectively two-dimensional (2D) quantum dots realized in semiconductor heterostructures [7] where electrons occupy well defined discrete levels that can be probed by Coulomb-blockade measurements [8]. The size of the sample can even be made smaller than the phase-coherence length of the system. These samples are referred to as ballistic. Consequently, in the spirit of quantum chaos, the geometry of the quantum dot becomes important as the wavefunctions and energy eigenstates depend sensitively on the geometry of the system's boundary due to self-interference effects [9, 10]. This new aspect, besides the much smaller number of electrons in the conduction band, has to be contrasted to Bloch waves in metals. The existence of mesoscopic fluctuations is another feature that governs the behaviour of such systems. All these differences from bulk systems have made mesoscopic systems an interesting object of research in the context of AOC and FES [11, 12, 13, 14, 15].

Here, we focus in particular on yet another difference from the bulk case that can easily be realized in mesoscopic structures, namely, the existence of degenerate energy levels (shells): Quantum dots with a few up to few hundred electrons are often very well described by a parabolic confining potential [16] that leads, in close analogy to the harmonic oscillator, to the organisation of

---

\*Electronic address: swarnali.bandopadhyay@ntnu.no

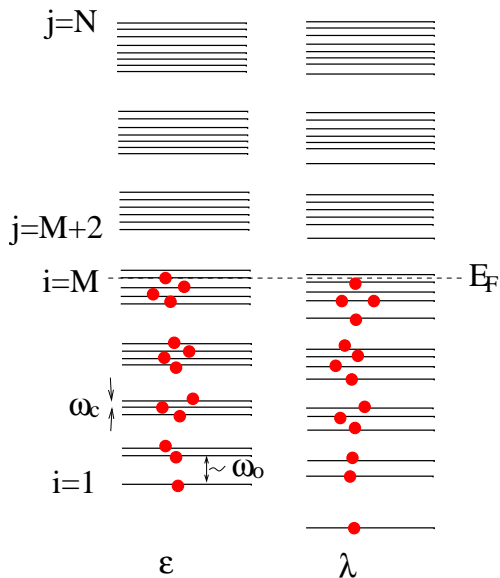


FIG. 1: A schematic diagram of the energy levels ( $\varepsilon$ ) in a PQD in the presence of a small magnetic field (characterised by cyclotron frequency  $\omega_c$ ) that slightly lifts the degeneracy of the PQD's energy-levels. Notice the shell structure. An attractive perturbation ( $V_c$ ) due to a core hole shifts the levels downwards and results in perturbed levels  $\lambda$ .  $M$  is the number of occupied dot levels (to the Fermi energy  $E_F$ ) and  $N$  is the total number of levels.

the energy levels in shells (see Fig. 1). The objective of the present paper is to study AOC in the presence of degeneracies and shell structures as they occur in realistic, parabolic quantum dots where, furthermore, an external magnetic field can be used to control the lifting of degeneracies. We show that the presence of shells considerably alters AOC of the system and leads to deviations from the power-law behaviour observed in the bulk systems.

The paper is organised as follows. In Sec. II we describe our model that follows the Fermi golden rule approach to FES in the x-ray edge problem introduced by Ohtaka and Tanabe in Refs. [5, 17]. The sudden, local perturbation

arising from the core hole is modelled as a rank-one perturbation. In Sec. III we present our results for AOC in parabolic quantum dots. First, we focus on the role of shell effects and neglect the dependence of the perturbation strength on the position of the perturbation. We then turn to the more realistic case where the dependence of the perturbation strength on the position, induced by the non-homogeneous electron intensity in PQD, as well as mesoscopic fluctuations are taken into account. For each case we consider both weak and strong magnitude of attractive perturbation and a weak magnetic control. Finally we draw conclusions in Sec. IV.

## II. THE MODEL

We start with a discussion of the energy levels and wavefunctions of the (unperturbed) PQD, paying special attention to the degeneracy of levels and their organisation in shells as this has crucial impact on the Anderson overlap. Its calculation is discussed in the second subsection.

### A. Energy levels and wave functions of the parabolic quantum dot

We describe the unperturbed system by the Hamiltonian

$$\hat{H}_0 = \sum_{k=0}^{N-1} \epsilon_k c_k^\dagger c_k \quad (1)$$

where the operator  $c_k^\dagger$  ( $c_k$ ) creates (annihilates) a particle in the unperturbed eigenstate  $\psi_k(\vec{r})$  with eigenenergy  $\epsilon_k$ .

A very weak magnetic field will be applied to lift the inherent degeneracy in the PQD energy levels. Tuning the strength of the applied field, characterised by the cyclotron frequency  $\omega_c$ , we can study quasi-degenerate to non-degenerate limits. In presence of a magnetic field, the eigenfunction and the corresponding eigenenergies of the PQD are [16]

$$\psi_{n,l}(r, \phi) = \frac{e^{il\phi}}{\sqrt{2\pi}l_b} \sqrt{\frac{n!}{(n+|l|)!}} \exp\left(-\frac{r^2}{4l_b^2}\right) \left(\frac{r}{\sqrt{2}l_b}\right)^{|l|} L^{|l|}\left(\frac{r^2}{2l_b^2}\right) \quad (2)$$

$$\epsilon_{n,l} = (2n + |l| + 1) \hbar (\omega_0^2 + \frac{1}{4} \omega_c^2)^{1/2} - \frac{1}{2} l \hbar \omega_c, \quad (3)$$

where  $\omega_0$  is the oscillator frequency ( $\omega_0 = 3meV$  for GaAs) and  $\omega_c = \frac{\hbar e B}{m^*}$  is the cyclotron frequency (with the effective mass  $m^* = 0.067 m_e$  for GaAs). The resulting characteristic frequency of the oscillator is  $\Omega = (\omega_0^2 + \frac{1}{4} \omega_c^2)^{1/2}$ . Furthermore,  $n (= 0, 1, 2, \dots)$  is the radial quantum number and  $l (= 0, \pm 1, \pm 2, \dots)$  is the

angular momentum quantum number.  $l_b (= \sqrt{\frac{\hbar}{m^* \Omega}})$  is the characteristic length of the oscillator.  $L_n^{|l|}(x) = \sum_{i=0}^n (-x)^i \frac{(n+|l|)!}{(n-i)! (|l+i|! i!)}$  is the generalised (associated) Laguerre polynomial. We use units  $\hbar = 1, m^* = 1, \omega_0 = 1$  in the following. We will consider PQDs with a to-

tal number of shells (“clusters”)  $S(= 2n + |l| + 1) = 1, 2, \dots, 50$ . Neglecting spin degrees of freedom, the  $p$ -th cluster contains  $p$  levels (Fig. 2).

The energy gap between two adjacent clusters is defined as the difference between the top-most level of the lower ( $i$ -th) cluster and the lowest level of next higher ( $i + 1$ )-th cluster, i.e.,

$$\Delta\epsilon = [(i + 1) - i]\Omega - \frac{1}{2} \left( \left| l_{\max}^{(i+1)} \right| + \left| l_{\max}^{(i)} \right| \right) \omega_c \quad (4)$$

Using  $\left| l_{\max}^{(i)} \right| = (i - 1)$  in Eq. (4), we find  $\Delta\epsilon = \Omega - (i - 1/2)\omega_c$ . Thus for given  $\omega_0$  and  $\omega_c$  with  $\omega_c \ll \omega_0$ ,  $\Delta\epsilon$  decreases for higher clusters.

Figure 2 shows the unperturbed levels as expressed in Eq. (3) for few values of  $\phi_c/\phi_0$  (upper panel). For small  $\phi_c/\phi_0$ , i.e., in the quasi-degenerate limit all the clusters are well-separated from their neighbours. With increasing  $\phi_c/\phi_0$ , levels from adjacent clusters start to mix in, eventually destroying the shell structure. For higher (and therefore larger) clusters, mixing starts for comparatively weaker  $\omega_c$  than for smaller clusters. For example, in Fig. 2, for  $\omega_c = 0.1\omega_0$  there is no mixing up to the tenth cluster, whereas for  $\omega_c = 0.5\omega_0$  mixing starts from third cluster. In the inset, we have plotted the sorted unperturbed levels of our system. Clustering of levels at weak  $\omega_c$  fades away with the increasing magnetic control parameter. For  $\omega_c = 0.5\omega_0$ , levels are almost equi-spaced. In the lower panel of Fig. 2, we have shown the energy difference of adjacent levels as a function of level index and magnetic control parameter. For small  $\omega_c$  ( $\simeq 0.1\phi_0$ ), in the absence of mixing, the energy separation between two adjacent clusters is constant and given by  $\Delta\epsilon \sim \phi_0$  with an intra-cluster level spacing of  $\Delta\epsilon_{ic} \sim \phi_c$ . With increasing  $\omega_c$ , as levels from different clusters start to mix in, the energy-spacing becomes a complicated function of  $\omega_0$ ,  $\omega_c$  and the cluster size. For certain ranges of  $\omega_c/\phi_0$  (e.g., around  $\phi_c/\phi_0 = 0.7$ ) one obtains an almost uniform level spacing. If one increases  $\omega_c$  further, levels start to form clusters again. However, these clusters are very different from the initial shell structure.

In the absence of a magnetic field, one can estimate the effective radius  $r_{\text{eff}}$  of the PQD by equating the energy  $\frac{1}{2} m^* \omega_0^2 r_{\text{eff}}^2$  at the classical turning point to the energy of the highest filled shell [16]. For a PQD with 15 shells and half-filling, i.e., a partially filled eleventh shell, corresponding to an energy  $\sim 11 \hbar \omega_0$ , the effective radius is  $r_{\text{eff}} = \sqrt{2} \times 11$  (which is  $4.7 \times 10^{-7} m$  for the above-mentioned GaAs quantum dot).

## B. Calculation of the Anderson overlap

Following the approach by Tanabe and Ohtaka [5, 17], we model the localised perturbation, generated by the sudden appearance of the core hole left behind after x-ray excitation of one core electron, as a local potential described as rank-one perturbation. For details of the

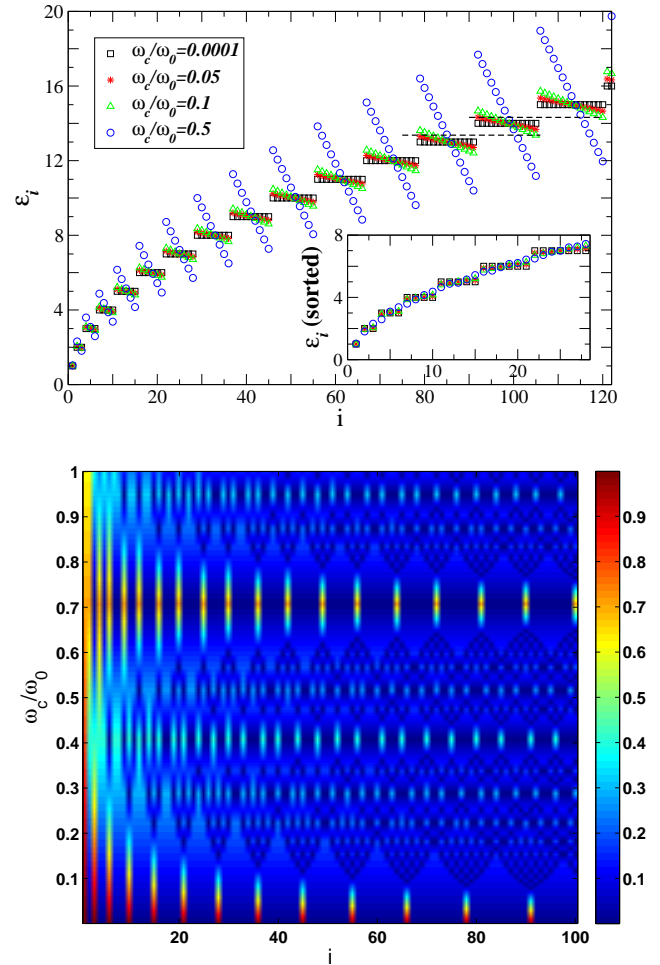


FIG. 2: (Color online) Upper panel: Energy  $\epsilon_i$  of the first  $i = 1, 2, \dots, 120$  unperturbed levels of a PQD with fixed total number of levels  $N = 250$  and fixed  $\omega_0 = 1$  for four different  $\omega_c$ . The shell (“cluster”) structure is clearly visible. For higher shells, mixing between adjacent clusters starts at lower  $\omega_c$ . Two dashed lines are shown as guide for the eye to indicate mixing at  $\omega_c/\phi_0 = 0.1$ . The inset shows the energy-sorted levels. Lower panel: The separation between two adjacent levels  $\delta\epsilon_i = \epsilon_{i+1} - \epsilon_i$  of the same PQD is shown as a color plot as a function of magnetic control  $\omega_c/\omega_0$  and energy level  $i$ . Note that a new shell structure forms near  $\phi_c/\phi_0 = 0.7$ .

underlying theory we refer the reader, e.g., to Refs. [5], [14] or [17]. The great advantage of a rank-one perturbation is that all quantities of interest can be expressed in terms of the unperturbed and perturbed energy levels (which, however, depend on the wave-function amplitude at the position of the perturbation; see Eq. (A1) in the appendix). Nevertheless it was found to provide a very reasonable description of the many-body effects contributing to the x-ray edge problem [5].

We write the rank-one contact potential as

$$\hat{V}_c = V_c \Omega_D f^\dagger(\vec{r}_c) f(\vec{r}_c), \quad (5)$$

with  $f(\vec{r}_c) = \sum_k \psi_k(\vec{r}_c) c_k$ , that acts only at the location

$\vec{r}_c$  of the core hole.  $\Omega_D$  is the volume of the PQD and the parameter  $V_c$  defines the strength of the potential. Note that its effective strength depends also on  $\psi_\kappa(\vec{r}_c)$ , i.e., on the amplitude of the wave function at the position of the perturbation. A small wave-function amplitude at  $\vec{r}_c$  will reduce the effective perturbation strength felt by the system. The energy levels  $\epsilon$  will move under the influence of  $\hat{V}_c$ , downward for an attractive potential (core hole) and upward for a repulsive one. We focus on an attractive perturbation  $V_c < 0$  (core hole) in what follows.  $V_c$  introduces a new energy scale into the problem, and  $V_c/\omega_0$  and  $\omega_c/\omega_0$  are the two dimensionless energy-scales of the PQD that govern the system's behaviour.

Introducing  $d_\kappa^\dagger$  as creation operator of a particle in the perturbed orbital  $\phi_\kappa$ , we can write the perturbed Hamiltonian in diagonal form as

$$\hat{H} = \hat{H}_0 + \hat{V}_c = \sum_{\kappa} \lambda_{\kappa} d_{\kappa}^{\dagger} d_{\kappa}. \quad (6)$$

To obtain the perturbed single particle states  $\phi_\kappa$  and their eigenvalues  $\lambda_\kappa$ , we diagonalise the total Hamiltonian  $\hat{H}$ . The unperturbed and perturbed many-body ground states for  $M$  electrons are obtained as Slater determinants,  $\Psi_0 = |\psi_1, \psi_2, \dots, \psi_M|$  (unperturbed) and  $\Phi_0 = |\phi_1, \phi_2, \dots, \phi_M|$  (perturbed). The Anderson overlap of these two many-body states is given by  $|\Delta|^2 = |\langle \Phi_0 | \Psi_0 \rangle|^2$ , with  $\Delta = \det(A)$ . The matrix elements of  $A$  are obtained by expanding each perturbed orbital in the basis of unperturbed orbitals. It can also be written in terms of the unperturbed and perturbed energy levels [5, 14].

According to the Friedel sum rule, the change in phase upon scattering at the local potential is related to the energy shift between the unperturbed and perturbed energy levels [25]. We therefore introduce the local phase shift for the level  $i$  (with  $i = M$  at the Fermi energy) as a measure of the rearrangement of levels due to the perturbation as

$$\phi_i = \pi \frac{\lambda_i - \epsilon_i}{\epsilon_i - \epsilon_{i-1}}.$$

Here, we have assumed  $V_c < 0$ . Similarly, for  $V_c > 0$  we find  $\phi_i = \pi (\lambda_i - \epsilon_i) / (\epsilon_{i+1} - \epsilon_i)$ .

### III. RESULTS

#### A. AOC in the presence of degeneracies: Deviations from the Anderson power law

First, we focus on the role of degeneracies on AOC. We therefore neglect the spatial dependence of the potential strength, i.e., we assume uniform amplitudes for all unperturbed orbitals throughout the PQD. To this end we consider a PQD subject to a very weak magnetic field with frequency  $\omega_c \ll \omega_0$  such that the degeneracies in energy space are just lifted, but the shell structure is kept

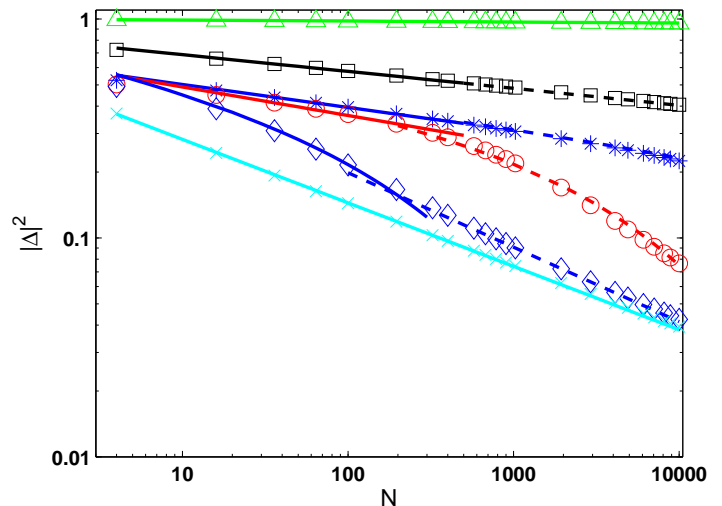


FIG. 3: (Color online) Many-body overlap  $|\Delta|^2$  as a function of system size  $N$  for six different strengths of perturbation. Points are obtained from the numerical evaluation of the Anderson overlap  $|\Delta|^2$ : the different points  $\Delta, \square, *, \circ, \diamond$  and  $\times$  are for  $|V_c|/\omega_c = 0.1, 1, 10, 100, 1000$  and  $10^5$  respectively. The solid and dashed curves represent the different functional form of  $|\Delta|^2$  obtained from analytics. The solid curves through  $\Delta, \square, *, \circ$  points are of the form  $N^{-0.5\delta^2/\omega_c^2}$  and well approximate the independent cluster regime (small  $|V_c|/\omega_c$  and/or small  $N$ ). Here  $0 < \delta/\omega_c < 1$  denotes the shift in energy levels (phase shift) inside the last filled cluster. For  $\Delta$ , the perturbation being very weak (cf. case (a) in the text), even for larger system size the power law behaviour survives. For other three cases the power-law decay gets enhanced in presence of exponential decay  $\exp(-\frac{3}{2}p^2\sqrt{N})$  in the large  $N$  limit. Here  $0 < p < 1$  is the measure of energy shift of the boundary levels in clusters. The  $\diamond$  points show exponential decay even for small system size. In this case, for large  $N$  limit, overlap follows  $N^{-\delta^2/\omega_c^2}$ . Finally, a strong perturbation, case (b) in the text, yields the solid curve through  $\times$  points,  $N^{-\delta^2/\omega_c^2}$ , and the Anderson power-law is recovered. Note that both  $\delta$  and  $p$  increase with  $|V_c|$ . For  $|V_c|/\omega_c = 0.1, 1, 10, 100, 1000$  and  $10^5$  the power law exponents are  $\delta^2/\omega_c^2 = 0.009(\phi = 0.095\pi), 0.18(\phi = 0.43\pi), 0.19(\phi = 0.44\pi), 0.21(\phi = 0.46\pi), 0.026(\phi = 0.51\pi)$  and  $0.26(\phi = 0.51\pi)$  respectively. For  $|V_c|/\omega_c = 1, 10, 100, 1000$  the coefficient of  $\sqrt{N}$  in argument of the exponential functions are  $\frac{3}{2}p^2 = 0.00005, 0.0008, 0.0112, 0.05$  respectively. Here we have chosen the magnetic control parameter  $\omega_c = 0.0001\omega_0$ .

intact. We will refer to it as PQD in quasi-degenerate limit.

For numerical calculations we have considered a PQD with a fixed number of shells  $S$ , i.e., a total number  $N = \frac{S(S+1)}{2}$  of levels with the lowest  $M$  levels being occupied. Hereon, we will refer to  $M/N$  as ‘filling’ of the PQD. In what follows, unless specified otherwise, we have chosen a PQD with a total number of shells  $S = 15$ , i.e., total number of levels  $N = 120$ . All energies are measured in units of  $\phi_0$  ( $\hbar = 1$ ).

In Fig. 3 we show the behaviour of overlap  $|\Delta|^2$  as a function of system size  $N$  for six different  $|V_c|$  keeping  $\phi_c$  and  $\phi_0$  fixed. We consider half-filled systems and  $N$  such that the Fermi cluster is half-filled as well. In contrast to Anderson’s result of a power-law decay of  $|\Delta|^2$  as a function of  $N$  for the bulk system, we find three different regimes in the presence of degeneracies (quasi-degenerate limit) in the quantum dot. Depending on the strength of  $|V_c|$ , we observe (Fig. 3):

(a)  $|V_c|$  very small – single cluster regime:  $|V_c|$  is so small that the separation between the clusters remains large even after the perturbation is applied. The many-body overlap is dominated by the rearrangement of levels in the last filled cluster (i.e., the shell at the Fermi energy, the *Fermi cluster* in short). Thus we can approximate the response of the whole system by that of the Fermi cluster, which itself acts like a harmonic oscillator. If  $s_M$  is the size of this cluster, the Anderson overlap is known [5, 14] to be  $|\Delta|^2 \sim s_M^{-(\phi/\pi)^2}$  where  $\phi$  is the phase shift at the Fermi energy. It is easy to see that for a half-filled parabolic dot with in total  $N$  levels, a half-filled Fermi cluster yields  $s_M = \sqrt{N}$ . Thus  $|\Delta|^2 \sim N^{-0.5(\phi/\pi)^2}$ . See the topmost two curves for small  $|V_c|/\omega_c$  in Fig. 3.

(b)  $|V_c|$  large – whole system responds:  $|V_c|$  is so large that the shells mix and the whole system participates in the response. For large  $|V_c|$ , the inter-cluster separation decreases to become comparable with intra-cluster level-separation. Then the energy levels of all shells participate in AOC response. In this regime we find the well-known result for the power-law decrease of the Anderson overlap, i.e.,  $|\Delta|^2 \sim N^{-(\phi/\pi)^2}$ .

(c)  $|V_c|$  intermediate – transition regime: In this regime the results will depend crucially on the system size  $N$  in addition to  $|V_c|$ . The gap between adjacent clusters decreases for bigger clusters, triggering the response of the whole system rather than a single shell. In addition, neighbouring clusters come closer to each other with increasing perturbation strength. This generates essentially the following sub-regimes in dependence on  $N$  (assuming  $|V_c|$  intermediate and constant):

(c-i) Small  $N$ : The separation between clusters is relatively large and one can again approximate the behaviour of the many body overlap of the whole system with that of the last partially (half-) filled cluster; thereby getting back to the result for independent clusters as in the case (a) for small  $|V_c|$ :  $|\Delta|^2 \sim N^{-0.5(\phi/\pi)^2}$ .

(c-ii) (Very) large  $N$ : For sufficiently large  $N$ , the clus-

ters are close enough to each other such that all of them contribute in the many-body overlap and give rise to the Anderson power law in this regime, similarly to case (b). In Fig. 3, the many-body overlap for  $|V_c|/\omega_c = 1000$  follows  $N^{-0.5(\phi/\pi)^2} \exp(-3p^2\sqrt{N}/2)$  in the small  $N$  regime and decreases as  $|\Delta|^2 \sim N^{-(\phi/\pi)^2}$  with  $N$  for larger systems. Note that the local phase-shift  $\phi = \pi \frac{\epsilon_M - \lambda_M}{\epsilon_M - \epsilon_{M-1}}$  at the Fermi energy is same for both  $|V_c|/\omega_c = 1000$  and  $|V_c|/\omega_c = 10^5$ , although the overlap exhibits a very different power-law behaviour. The local phase-shift does not contain any information about the participating clusters. As a result, phase-shift becomes insufficient to fully describe the many-body overlap in PQDs. This, again, contrasts the behaviour known in bulk (metallic) systems (see [22]) where the phase shift at the Fermi energy alone is known to determine the overlap.

(c-iii) Intermediate  $N$ : The overall behaviour is more complicated and characterised by the transition between the cases (c-i) and (c-ii). To gain a deeper, quantitative understanding, we have performed an explicit analytic calculation assuming that the last occupied shell is half filled and that this cluster and its two neighbouring clusters (one filled and the other empty) determine the behaviour of the many body overlap. This calculation is outlined in Appendix A and yields the result  $|\Delta|^2 \sim N^{-0.5(\phi/\pi)^2} \exp(-3p^2\sqrt{N}/2)$ . The solid curve through  $\diamond$ -points in Fig. 3 is provided by this expression. It well reproduces the overlaps in the transition regime, before the Anderson power law takes over again in large  $N$  regime.

To summarise the effect of the shell structure on the Anderson overlap for intermediate  $|V_c|$  (cf. the third, fourth curves from top in Fig. 3), we expect the small  $N$  regime with  $|\Delta|^2 \sim N^{-0.5(\phi/\pi)^2}$  to cross over to an regime with  $|\Delta|^2 \sim N^{-0.5(\phi/\pi)^2} \exp(-3p^2\sqrt{N}/2)$  for intermediate to large  $N$ . Increasing  $|V_c|$  further, the clusters start to mix even for small system size. In Fig. 3, for  $|V_c|/\omega_c = 1000$ , the many-body overlap  $|\Delta|^2 \sim N^{-0.5(\phi/\pi)^2} \exp(-3p^2\sqrt{N}/2)$  in the small  $N$  regime. In the limit of very large  $N$  the Anderson power law  $|\Delta|^2 \sim N^{-(\phi/\pi)^2}$  is recovered. Note that for intermediate strength of perturbation decay rate of many-body overlap with system size could be faster than in case of stronger perturbation. This change in power law is due to the number of participating clusters in the many-body overlap, note that the phase shift  $\phi$  at the Fermi energy itself does not change. This behaviour marks a clear deviation from the well-known Anderson result [1] for bulk systems that was also found to hold for other (chaotic) mesoscopic systems [11, 12, 13, 14]. It is a consequence of the shell structure, i.e., the degeneracy of energy levels. Since this can be easily realized in the mesoscopic regime by using the well-established semiconductor-heterostructure parabolic quantum dots, this interesting behaviour becomes accessible to experiments.

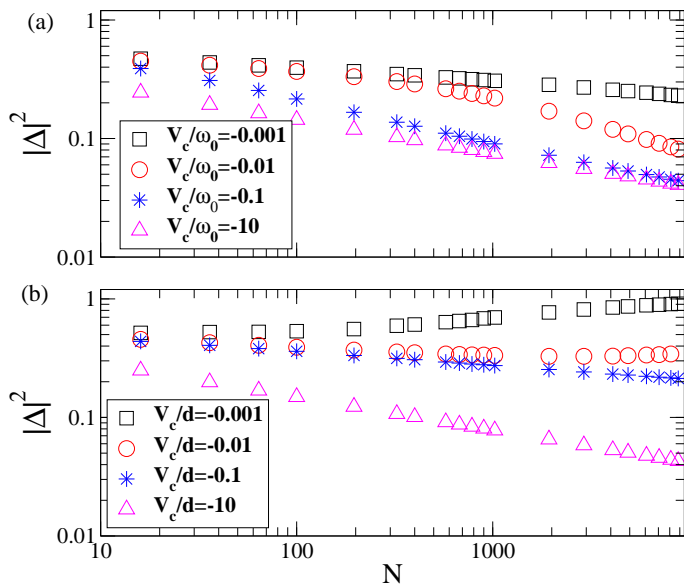


FIG. 4: (Color online) (a) Manybody overlap  $|\Delta|^2$  as a function of system size  $N$  for 4 different strength of perturbation scaled with oscillator's frequency  $\phi_0$  is compared with (b)  $|\Delta|^2$  as a function of system size  $N$  for four different strengths of perturbation scaled with average level spacing  $d$ .

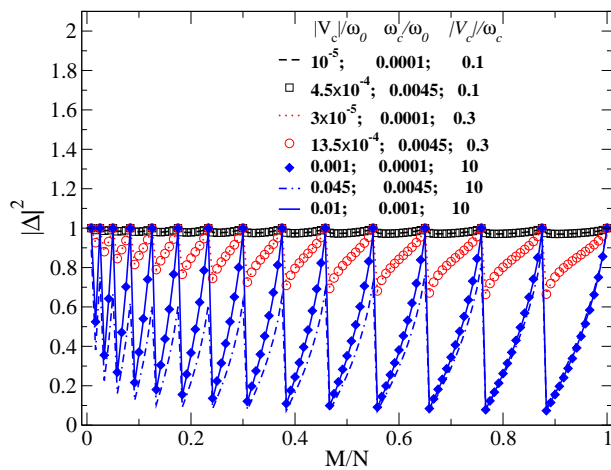


FIG. 5: (Color online) Many-body overlap  $|\Delta|^2$  for a PQD is shown as a function of filling  $M/N$ . In the regime of weak magnetic field ( $\omega_c < 0.01\omega_0$ ) and weak perturbation  $V_c \leq 0.01\omega_0$ , the magnitude of overlap remains same for the same ratio of  $|V_c|/\omega_c$ .

## B. Shell effects in AOC

Another illustration that highlights the role of shells and the  $|V_c|$ -dependent inter-shell spacing is shown in Fig. 4. We consider  $|\Delta|^2(N)$  for different  $|V_c|$  that are scaled with respect to the inter-shell spacing measure  $\phi_0$  in Fig. 4(a) and with respect to the mean level spacing  $d$  (defined using only the levels in occupied clusters,

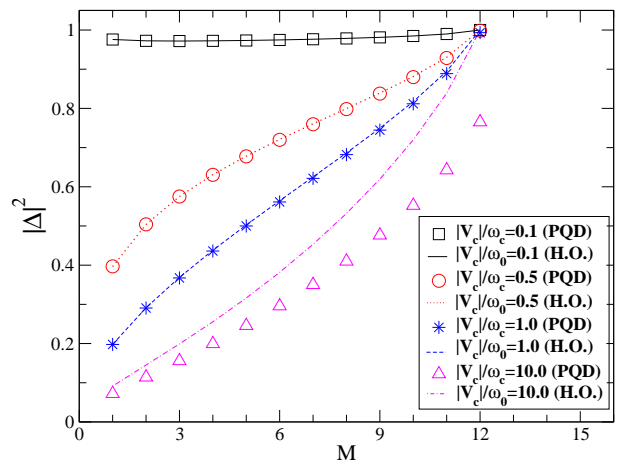


FIG. 6: (Color online) Many-body-overlap  $|\Delta|^2$  as function of number of electrons  $M$ . The 12-th cluster of a PQD with 15 shells (symbols) is compared with  $|\Delta|^2$  of a 1D harmonic oscillator (HO) having 12 energy levels with level spacing  $\phi_c$  (lines). The PQD is characterised by  $\omega_c = 0.0045\phi_0$ , and  $M$  refers to the number of electrons in the 12th shell. Deviations between the two curves occur away from the small  $V_c/\phi_c$  limit.

$d = 2\Omega/s_M$  in the large dot limit) in Fig. 4(b). The motivation behind is a scaling of the Anderson overlap with  $|V_c|/d$  that was reported in Refs. [13, 14]. For intermediate perturbation strength (squares in Fig. 4),  $|\Delta|^2$  decreases with  $N$  in (a) but increases with  $N$  in panel (b) in the large cluster limit. Since  $d$  is inversely proportional to  $\sqrt{N}$ , for larger clusters to keep the ratio  $|V_c|/d$  constant one needs to apply a weaker perturbation. This generates a larger many-body overlap with increasing system size. Consequently, the scaling of physical quantities with  $|V_c|/d$  that was found to be characteristic for other (chaotic) mesoscopic systems, can be completely overtaken by the shell structures in PQDs.

The possibility to precisely control the number of electrons on quantum dots through Coulomb blockade motivates us to study the many-body overlap  $|\Delta|^2$  as a function of filling  $M/N$ , where  $M$  is the number of filled energy levels and  $N$  is the total number of energy levels considered. The results obtained in the quasi-degenerate limit are shown in Fig. 5. We consider very weak perturbations ( $|V_c| \leq 0.01\phi_0$ ) and tune  $|V_c|$  and the magnetic control field  $\omega_c$ . From Fig. 5, one can see that changing  $|V_c|$  and  $\phi_c$  keeping the ratio  $|V_c|/\phi_c$  constant generates the same magnitude of overlap at a given filling  $M/N$ , i.e., a scaling behaviour of  $|\Delta|^2$  holds for small  $|V_c|/\phi_c$ . The shell structure with 15 distinct clusters is easily visible in Fig. 5. The overlap reaches 1 at the completion of each cluster; as the adjacent clusters - for the small  $|V_c|$  considered here - are widely separated in energy and do not contribute. Note that the overlap drops to a *small* value whenever a new shell is opened, even for the *weak*  $|V_c|$  considered here. The reason is the larger size of the available phase space for shells with small filling. The drop in the many-body overlap at the opening of a new

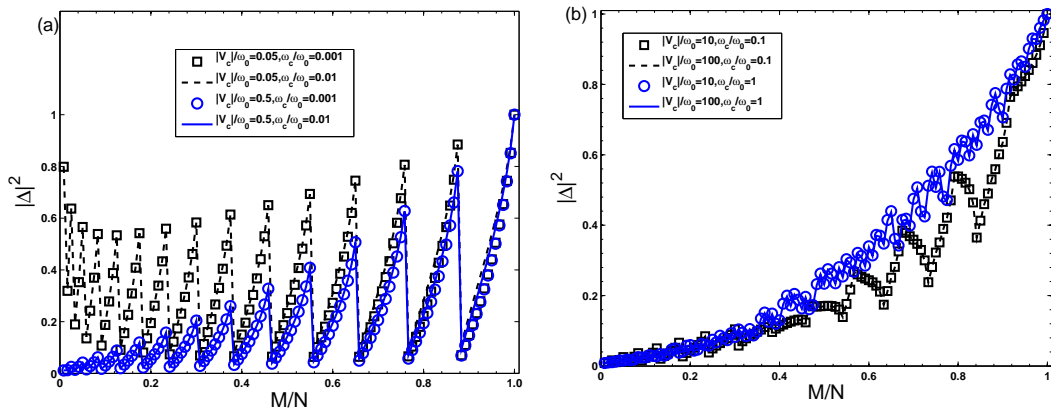


FIG. 7: (Color online) Many-body overlap  $|\Delta|^2$  for a PQD shown as a function of filling  $M/N$ . The results are obtained for (a) moderate perturbation  $|V_c| \geq 0.01\omega_0$  in the quasi-degenerate limit and (b) for strong magnetic field ( $\omega_c \geq 0.1\omega_0$ ) and strong perturbation  $|V_c| > 5\omega_0$ . In (a) the magnitude of  $|V_c|$ , determines the value of the overlap at all filling. In (b), behaviour of the overlap is controlled by  $\phi_c$ .

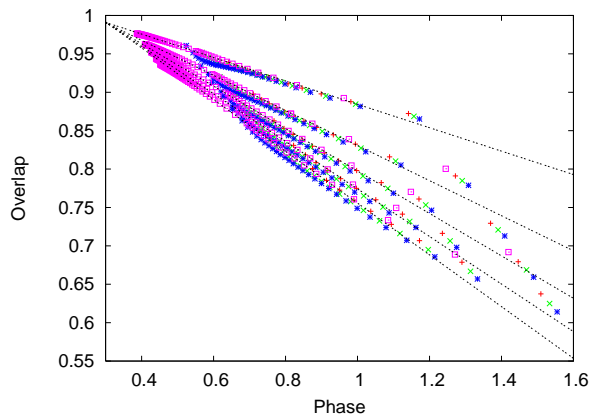


FIG. 8: (Color online) The many-body overlap as a function of phase shift for three different PQDs as well as for a number of 1D harmonic oscillators (HO). The different symbols are: PQD with 15 (+), 25 ( $\times$ ), 35 ( $*$ ) clusters and HOs with 1 up to 35 levels ( $\square$ ). The dashed lines are guide to the eye. From top to bottom, the five different curves correspond to clusters of a PQD and HOs with 1, 2  $\dots$  5 unoccupied levels, respectively. For the PQD, the magnetic control is chosen as  $\phi_c = 0.0001\phi_0$  the frequency of harmonic oscillator is  $\phi_c$ . All 4 systems are perturbed by an attractive perturbation of strength  $|V_c| = 0.0001\phi_0$ .

shell is a phase-space factor that - for sufficiently small perturbations - is given by the inverse of the level degeneracy. Details will be discussed elsewhere [26].

Interestingly, for weak perturbations ( $|V_c|/\omega_0 \leq 0.01$ , the quasi-degenerate limit) the many-body overlap  $|\Delta|^2$  of each cluster behaves independently and like an 1D harmonic oscillator (H.O.) of natural frequency  $\phi_c$  and the same number of levels as in the cluster in consideration subject to the same perturbation strength  $|V_c|$ , see Fig. 6. For the 1D harmonic oscillator, the natural frequency gives the measure of level-spacing whereas for PQD the

same role is played by the cyclotron frequency  $\phi_c$ . In this case, applying a weak magnetic field, the adjacent clusters of a PQD remain well separated in energy. The weak perturbation  $|V_c|$  shifts these clusters only slightly. As a result each cluster behaves independently or, in other words, the many-body overlap is determined by the last (partially) filled cluster alone.

In Figs. 5 and 6 we have focused on the case of weak perturbations and a small (control) magnetic field. We now increase the perturbation strength  $|V_c|$  to values that appear to be more realistic, e.g., in the context of photoemission- or photoabsorption-induced Fermi edge singularities (see Fig. 7). The chosen  $\omega_c$  scale has been increased a little such that it has a common  $\omega_c$  regime with Fig. 5. In this intermediate regime of perturbation, the shell structure response is somewhat modified, for example, now the overlap remains smaller than one even at the complete filling of a shell - a direct consequence of AOC. Note in particular that the overlap does not scale with  $|V_c|/\omega_c$  anymore, see Fig. 7(a). Rather, it is now determined by  $|V_c|$  alone (remember that we set  $\phi_0$  constant), and is *not* affected by changes of  $\phi_c$ .

Next we turn on a strong magnetic field such that clustering of energy space is broken partially or completely (see Fig. 7(b)), and also increase  $|V_c|$  further. With increasing  $\phi_c$  the levels in an unperturbed cluster start to spread apart from each other and eventually mix with levels from the neighbouring clusters. Accordingly, the shell structure in  $|\Delta|^2(N)$  is now (almost) lost, and the overlap shows an approximate monotonic increase with filling. In this regime, the behaviour of  $|\Delta|^2$  as a function of filling is solely determined by the magnetic field strength (characterised by cyclotron frequency  $\phi_c$ ). However a fine tuning of  $|\Delta|^2$  is possible by changing  $|V_c|$ .

It would be worthy to mention that again at around  $\phi_c = 0.7\phi_0$  which corresponds to a new clustering of unperturbed levels (see lower panel of Fig. 2 and the discussion there) all three distinct regimes of  $|\Delta|^2$  as a function

of filling can be observed over a wider span in  $|V_c|/\phi_c$  parameter space.

We close this subsection by a discussion of shell effects and the scaling behaviour observed in Fig. 5 in terms of phase shifts. It is well known that for metals, the AOC (and FES) response is fully characterised by the phase shift at the Fermi energy, through the Anderson power law [27]. Here we study the many-body overlap as a function of phase shift at the Fermi energy in the presence of shell structures (see Fig. 8). We have collected the many-body overlap from partially filled clusters of three different systems with 15, 25 and 35 shells, respectively, characterised by different symbols in Fig. 8 subject to a (very) weak perturbation (similar to Fig. 5). We have considered five different fillings for each shell, namely each shell contains 1, 2,  $\dots$ , 5 unoccupied levels. From Fig. 8, one can easily see that five different curves emerge from the collected data, each of them corresponds to a fixed number of unoccupied levels. As expected from Fig. 5, the overlap is larger for ‘almost filled’ shells and it decreases with the increasing number of empty levels. In each curve, the overlap increases with increasing size of clusters or filling of clusters. The dashed straight lines are a guide to the eye. This observed linearity is a manifestation of scaling behaviour of  $|\Delta|^2$  for constant  $|V_c|/\phi_c$  of a PQD subject to weak perturbation in the quasi-degenerate limit. For comparison, we have calculated overlap and phase-shift at Fermi energy for harmonic oscillators with 35 equidistant energy levels, among which 1, 2,  $\dots$ , 5 are empty. In this weak perturbation regime, as expected, the results (marked as boxes in Fig. 8) match with the five curves obtained for PQD. Note that the phase shift decreases as we go to higher clusters (i.e., higher fillings). Deviations from linearity occur as soon as the different clusters start to mix. Note that for a PQD with 15 shells ( $N = 120$ ) the mixing occurs at around  $\phi_c = 0.07\phi_0$ , whereas for a PQD with 25 shells ( $N = 325$ ) and 35 shells ( $N = 630$ ) mixing starts at much lower  $\phi_c$ . This is the reason that for the PQD with 15 shells linearity holds for all the clusters present in the system but for larger systems linearity breaks for the higher (and therefore larger) clusters.

### C. AOC in the mesoscopic case

So far we have focused on the impact of the shell structure on AOC and assumed constant wave-function amplitudes (as in the metallic case) throughout the PQD. Now we turn to the truly mesoscopic case, i.e., the position dependence of the wave-function amplitude at the point of perturbation will be taken into account.

First we consider a PQD with 15 shells (i.e.,  $N = 120$ ) under intermediate and strong perturbation applied at two different positions. We calculate the many-body overlap  $|\Delta|^2$  as a function of filling of the PQD, as before, in Figs. 5 and 7. The results are shown in Fig. 9. As before, here too, one can clearly identify the existence

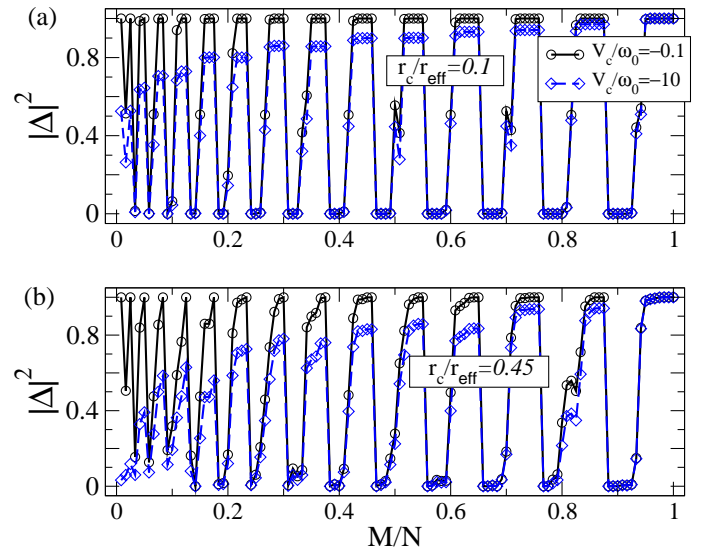


FIG. 9: (Color online) Many-body overlap  $|\Delta|^2$  as a function of filling  $M/N$  for a PQD with 15 shells ( $N = 120$ ) under intermediate (○) and strong (◇) perturbation applied (a) very close

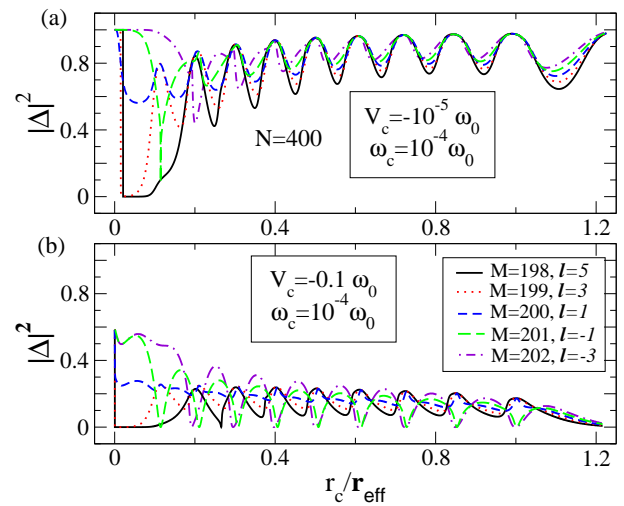


FIG. 10: Many-body overlap  $|\Delta|^2$  as a function of the position  $r_c$  of the perturbation for a PQD ( $N = 400$ ) around half-filling under (a) weak and (b) moderate attractive perturbation.

of the 15 shells in the dot. However, unlike the previous case, within a shell the overlap  $|\Delta|^2$  may now be non-monotonic function of filling and often forms a plateau at the shell boundaries. This saturation of the overlap is an interesting feature especially from the point of view of experimental studies.

Next we study how the Anderson overlap varies with position  $r_c$  of the localised perturbation. To this end we consider PQDs with  $N = 64$  and 400 around half-filling  $M/N = 1/2$  deep inside the quasi-degenerate limit and apply weak and moderate perturbations. Again,  $N$  is chosen such that for a half-filled system, the Fermi

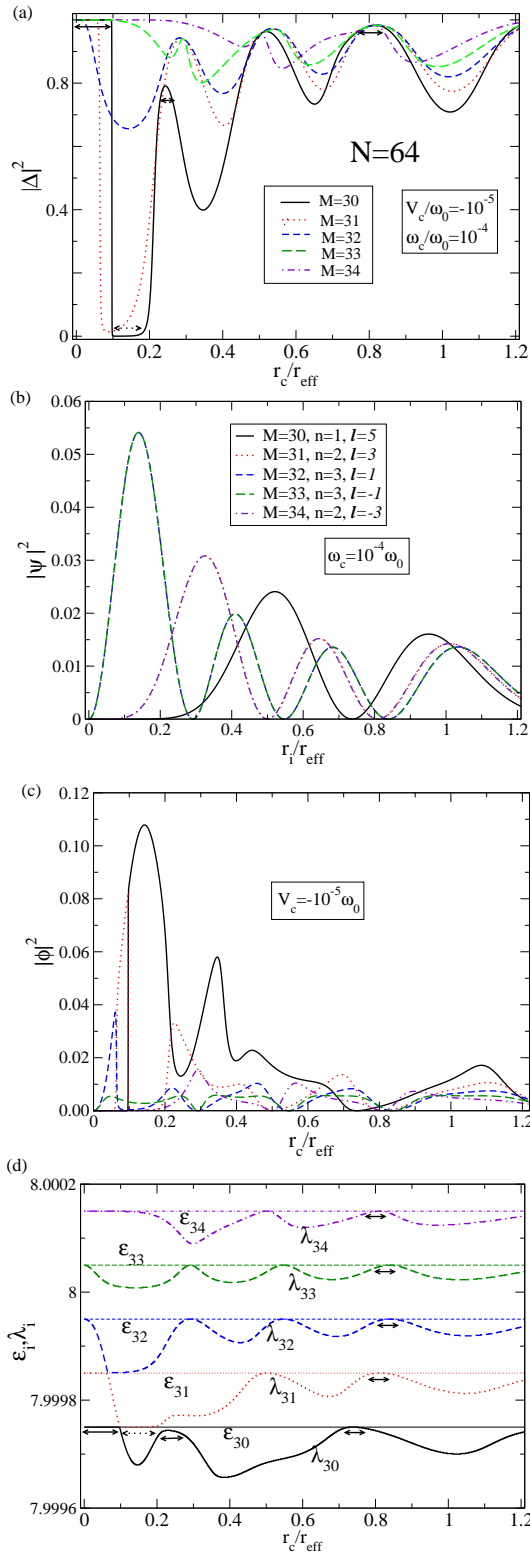


FIG. 11: (Color online) (a) Many-body overlap  $|\Delta|^2$  as a function of  $r_c$  for a PQD ( $N = 64$ ) around half filling ( $M = 32 \pm 2$ ) subject to a weak attractive perturbation. (b) Unperturbed orbitals as a function of radial distance  $r_i/r_{\text{eff}}$  from the centre of the same PQD. In (c) and (d) the amplitude of orbitals at the position of the perturbation and the corresponding perturbed energy levels are shown respectively. The straight lines in (d) mark the position of the unperturbed energies  $\epsilon_i$ . See text for details.

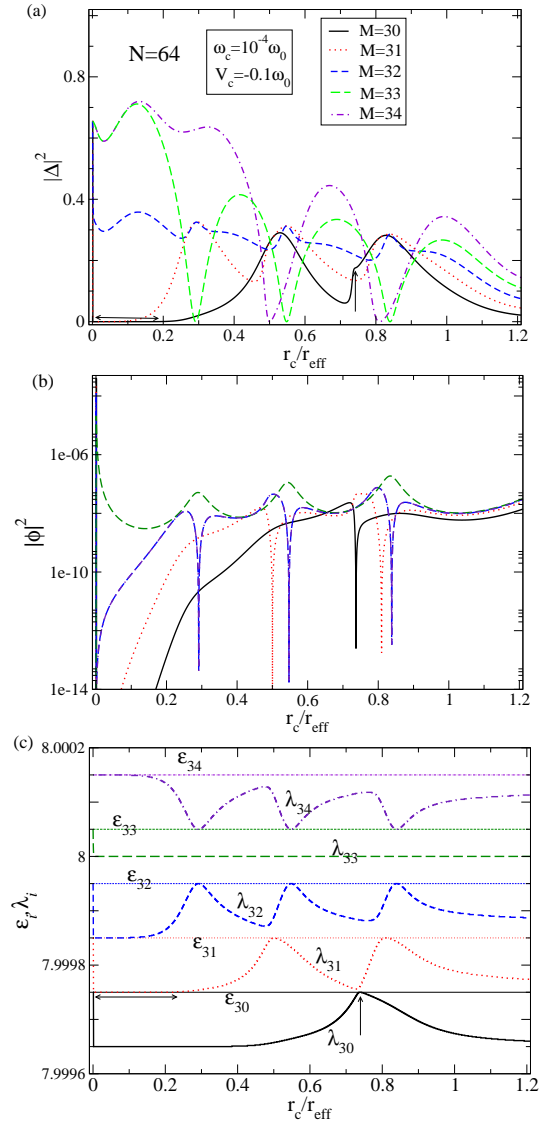


FIG. 12: (Color online) (a) Many-body overlap  $|\Delta|^2$  as a function of  $r_c$  for a PQD ( $N = 64$ ) around half filling ( $M = 32 \pm 2$ ) subject to an attractive perturbation of moderate strength. In (b) and (c), the amplitude of orbitals at the position of the perturbation and the corresponding perturbed energy levels are shown respectively. The horizontal straight lines in (c) mark the position of the unperturbed energies  $\epsilon_i$ .

cluster is also half filled. For the smaller  $N = 64$  (bigger  $N = 400$ ) dot the last partially filled cluster is the 8th (20th) cluster. We vary the position of the perturbation and calculate many-body overlap  $|\Delta|^2$  for given  $|V_c|$  and  $\varphi_c$ .

The result is shown in Fig. 10 for (a) a weak and (b) a moderately strong perturbation in the large dot ( $N = 400$ ). In both cases, the overlap varies with position  $r_c$  and shows strong dependence on filling  $M/N$ . These oscillations depend on the structure of the wave functions, in particular on the angular momentum quantum number  $l$ , as the effective perturbation felt by the system depends on the wave function amplitude at  $r_c$  around the Fermi energy, besides the strength of  $|V_c|$ . The value of  $l$  determines, in particular, the behaviour near the center of the dot. We discuss it in more detail below. The overlap is, as expected, smaller for the larger perturbation for most  $r_c$ . Note, however, that unlike the bulk (or bulk-like) case, even within a cluster, the overlap is not a monotonic function of filling (or,  $M$  for fixed  $N$ ).

To understand the oscillatory behaviour of the overlap, we have chosen a smaller dot with  $N = 64$  subjected to weak and intermediate perturbations in the quasi-degenerate limit, see Figs. 11 and 12 respectively. We consider again five fillings near the half filling. The corresponding highest filled unperturbed orbitals are shown in Fig. 11(b). They all have nodes at the centre, as  $l \neq 0$ , with a wider dip for larger  $l$ . The value of the perturbed orbital, at the position of the perturbation, is shown in Figs. 11(c) and 12(b). It illustrates the strong effect of the perturbation on the orbital intensity, especially near the dot-centre, as well as the differences between weak and intermediate perturbations. The lowest panels, in both the figures, show the perturbed single particle energies, again as a function of  $r_c$ .

The Anderson overlap  $|\Delta|^2$  in Figs. 11(a) and 12(a) can be understood by referring to Eq. A1. When  $\lambda_{M+1}$  equals to  $\epsilon_M$ , many-body-overlap  $|\Delta|^2$  goes to zero (indicated by dotted horizontal arrows near  $r_c = 0.15$  in Figs. 11(a) and 11(d)). On the other hand, when  $\lambda_M$  equals to  $\epsilon_M$ , the many-body overlap goes to 1. Similarly, when the unperturbed last filled level hardly changes after perturbation,  $|\Delta|^2$  shows a peak, marked by solid horizontal arrows in Fig. 11. Thus for weak perturbations, the filled and empty levels close to Fermi energy largely determine the many-body overlap. In the case of stronger perturbations (Fig. 12) the values for the overlap are smaller in general. When the last filled energy level coincides with the next higher perturbed level,  $|\Delta|^2$  goes to zero as before (marked by the solid horizontal arrows). However, in general the behaviour is more involved, note in particular the larger spread in the overlaps at a given  $r_c$ . Unlike the weak perturbation case, not only few levels close to Fermi-level are dominating the many-body overlap. Rather, more and more levels play a significant role in determining  $|\Delta|^2$ . In other words, the AOC many-body effect becomes more prominent with stronger

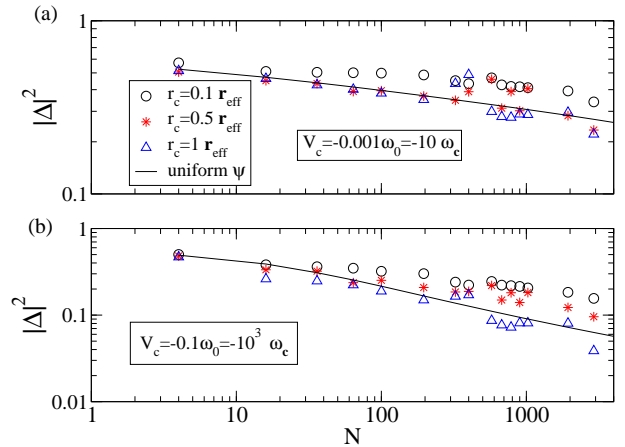


FIG. 13: (Color online) (a) Manybody overlap as a function of  $N$ . We consider half-filled clusters and half-filled systems. (b) For comparison, the overlap obtained for uniform amplitude is also shown.

perturbation. Note that the large fluctuations in  $|\Delta|^2$  as well as the spikes in  $|\phi|^2$  are related to the occurrence of avoided level crossings at the Fermi energy, one example is marked by the solid vertical arrow in Fig.12(c).

We now investigate the system size dependence of the many-body-overlap  $|\Delta|^2(N)$  for three different positions  $r_c$  of the perturbing potential. We consider half-filled systems with half-filled Fermi clusters, in order to avoid overshadowing effects that might have come from differences in shell-fillings. Two sets of results, obtained for two different  $|V_c|$ , are shown in Fig. 13. When the perturbing position is chosen close to the centre of the dot where most of the wave-functions (all with non-zero  $l$ ) have zero amplitude, the overlap is indeed somewhat larger than in the uniform amplitude case (see the open circles in Fig. 13). Applying the perturbation away from the dot centre, i.e., away from the centrifugal barrier (triangles and stars), makes the presence of mesoscopic fluctuations evident:  $|\Delta|^2$  shows a strong dependence on  $r_c$  at each  $N$ . Consequently, there are deviations from the uniform amplitude case keeping the qualitative nature unchanged. The deviations would be averaged out after averaging over a large number of realizations. Accordingly, the deviations from the Anderson power law exponent, discussed in Section III A, apply now to the averaged many-body overlap.

Now we focus on the mesoscopic fluctuations and discuss the probability distribution of overlaps  $|\Delta|^2$  for two systems around half filling (Fig. 14). We have chosen four different strengths  $|V_c|$  of attractive perturbation, its position  $r_c$  is assumed to be uniformly spread over the PQD and collected over 5000 different values to estimate the overlap distribution. Because of the circular symmetry of the PQD  $|\Delta|^2$  is independent of the angular positioning of the perturbation and depends only on  $r_c$ . For the weak perturbation case, as expected, the distribution  $P(|\Delta|^2)$  has a large peak near  $|\Delta|^2 = 1$  (see Fig. 14(a)).

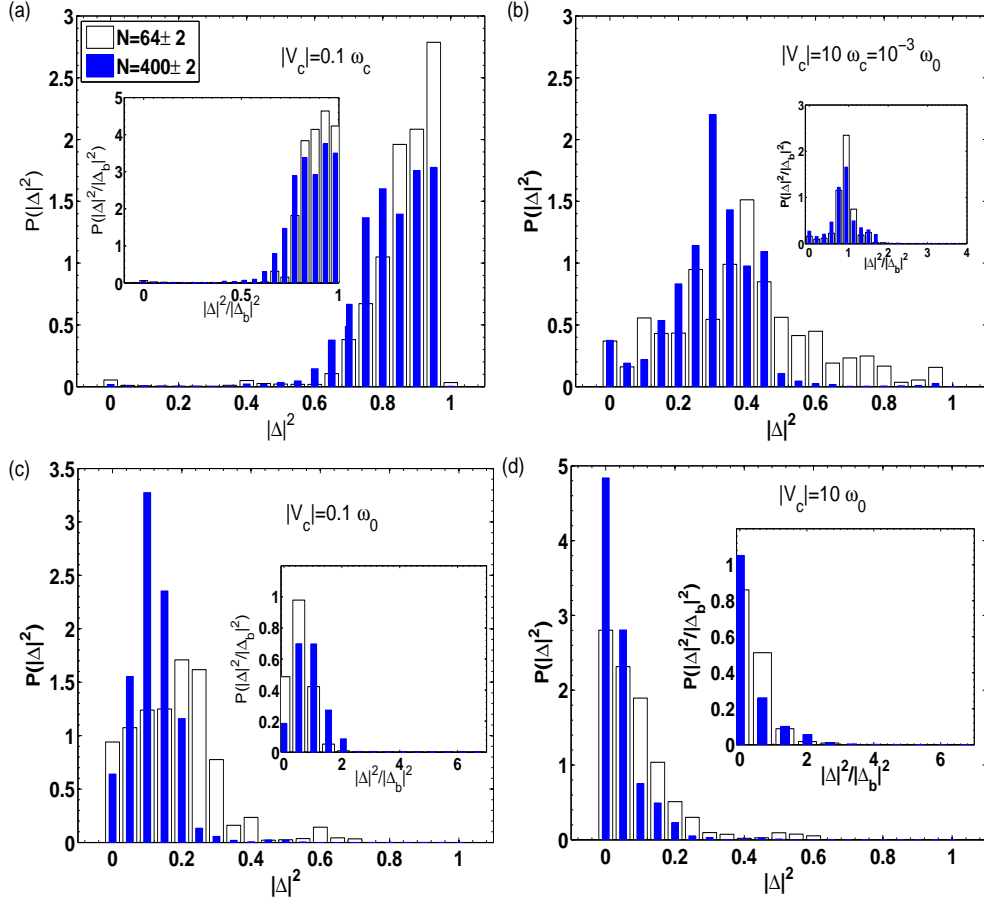


FIG. 14: (Color online) The distribution of many-body overlaps for two different PQD sizes (open and solid bars) and half-filled systems under (a) weak, (b) moderate, (c) strong, and (d) very strong attractive perturbation. To obtain the distribution, data were collected over 5 different  $M$  close to half-filling as well as 5 different values of  $N$  such that  $N \in [2M - 2, 2M + 2]$ . 5000 different  $r_c$  were chosen for each pair of  $M, N$ . We set  $\omega_c = 0.0001\omega_0$ . In the inset of each panel, the corresponding distribution of the overlap scaled by  $\Delta_b$  is shown. Here  $|\Delta_b|^2$  is the many-body overlap with uniform wave-amplitude in PQD.

Since, even for weak perturbation the overlap can be very small when a cluster is less than half filled, one can find a very small but finite probability for very small overlaps. Increasing the strength of the perturbation, the overlap distribution becomes even wider before reducing in width towards very strong perturbations. Getting a larger overlap becomes less and less probable and the peak is moved to smaller values (Fig. 14(b), (c) and (d)).

It is interesting to compare the distributions for  $N = 64$  and  $N = 400$ , e.g., in Fig. 14(b). The smaller system possesses the larger overlaps, as expected. If this is taken into account by scaling all results by the overlap  $\Delta_b$  of the corresponding PQD with uniform amplitude (see insets), the two probability distributions coincide much better, though not as good as in Refs. [13, 14].

Finally, we address the particle-hole symmetry of the Anderson overlap (see Fig. 15). We calculate the many-body overlap for few selected fillings in the 8-th cluster of a PQD with  $N = 64$  that are related by particle-hole symmetry. For not too large  $|V_c|$ , an electron in the

presence of an attractive perturbation and a hole in the presence of a repulsive perturbation represent the same thing physically. From Fig. 15, one can see that the overlap for a fixed number excess electrons (number of extra electrons from closest completely filled cluster) is mirror symmetric about  $V_c = 0$  to the overlap for a PQD with same number of holes (deficit in number of electrons to form a completely filled cluster). However, for stronger perturbations, when different clusters start to mix, the particle-hole symmetry does not hold. For bigger systems, as the mixing starts for weaker perturbation (as we have seen in Fig. 3) the asymmetry in many-body overlap appears for much smaller strength of perturbation. With increasing  $V_c$  (positive or negative),  $|\Delta|^2$  decreases. However, the reduction, beyond the symmetric regime of small  $V_c$ , is much steeper in the case of repulsive  $V_c$  than for attractive  $V_c$ .

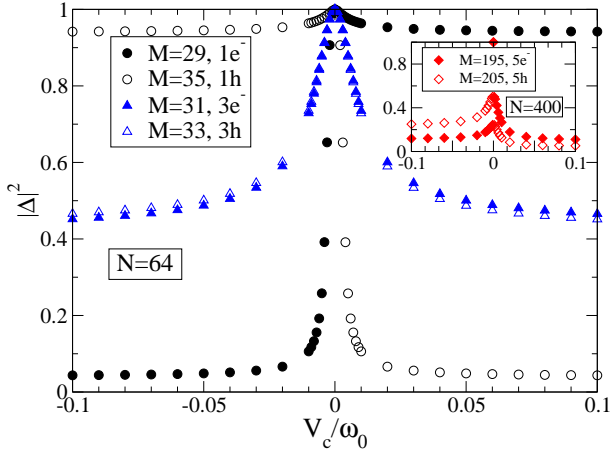


FIG. 15: (Color online) The many-body overlap as a function of perturbing potential strength  $V_c$  is shown for a few selected  $M$  chosen from 8-th cluster of a PQR having 64 levels in total. Here, the symbol  $e^-$  stands for extra (from nearest closed cluster) electrons,  $h$  for extra holes. We set  $\omega_c = 0.0001 \omega_0$  and  $r_c/r_{\text{eff}} = 0.5$ . In the inset, a pair of curves representing many-body overlap as a function of perturbing potential strength  $V_c$  are shown for a PQR with  $N = 400$  levels and  $M$  belong to 20-th cluster.

#### IV. CONCLUSION

We have studied the Anderson orthogonality catastrophe (AOC) for experimentally accessible parabolic quantum dots. Our results show that in addition to strength and position of the perturbation, level degeneracy and the rearrangement of shell structures are important in determining the behaviour of the many-body overlap.

As a reference system, we started with a simplified PQR with uniform amplitudes. For such a system, shell effects in the Anderson overlap are strong, especially in the quasi-degenerate limit. This shell effect survives in the mesoscopic case as well, even in presence of mesoscopic fluctuations. The rearrangement of energy levels between the shells leads to deviations from the well-known Anderson power law of the overlap. It is especially prominent for intermediate perturbation strengths when the power law behaviour of independent cluster approximation in small  $N$  regime gets modified by an exponential decay with system size in the large  $N$  regime (Fig. 3).

In the mesoscopic situation with position dependent wave-function amplitudes, the position of the perturbation strongly influences the Anderson overlap. We obtained a broad distribution of overlaps for various positioning of the localized perturbations. This distribution scales with the overlap  $|\Delta_b|^2$  obtained for a system with uniform amplitudes.

Our results underline the richness of samples in the mesoscopic regime with respect to many-body physics. In the present study, it is in particular the degeneracy of levels in parabolic quantum dots that makes AOC an interesting topic with new features that go well beyond

the well understood bulk metallic case.

#### APPENDIX A: POWER-LAW BEHAVIOUR OF THE OVERLAP IN DEPENDENCE ON PERTURBATION STRENGTH AND PARTICIPATING CLUSTERS

For a contact-type or rank-one perturbation, the many-body overlap can be expressed in terms of all single particle energy states [5] as

$$|\Delta|^2 = \prod_{i=1}^M \prod_{j=M+1}^N \frac{(\lambda_j - \epsilon_i)(\epsilon_j - \lambda_i)}{(\lambda_j - \lambda_i)(\epsilon_j - \epsilon_i)}. \quad (\text{A1})$$

Depending on the perturbation strength, the lowest level  $\lambda_0$  of a chaotic system gets shifted by a larger amount (“formation of a bound state”) than the other levels that are bound by their neighbors. For PQR, this scenario applies to the lowest level of each cluster that can be shifted more compared to all other levels of the cluster in application of the same perturbation. For example, the lowest level of Fermi cluster ( $s_M$ ) can have a shift of order  $p D_{s_M-1}$  with  $0 < p < 1$  and  $D_{s_M-1} = \omega_0 - s_M \omega_c + 3\omega_c/2$ , the energy gap with the neighbouring filled cluster ( $s_{M-1}$ ). All other levels of the cluster ( $s_M$ ) can be lowered by an amount  $q \omega_c$ , where  $0 < q < 1$  and  $\omega_c$  is the separation between adjacent levels in a cluster. Thus in the quasi-degenerate limit ( $\omega_c \ll \omega_0$ ) and for small PQR, the clusters remain well separated. Therefore we can confine our considerations to the contributions from levels deep inside the Fermi cluster to obtain many-body overlap. However, for very large clusters ( $s_M \rightarrow \infty$ ), all clusters are at comparable separations as their constituting levels. In this case, in addition to the Fermi cluster (with its lowest level being somewhat separated), we have to take into account the neighbouring clusters as well. To incorporate the distinctions between boundary levels and core levels in the expression of overlap in Eq. (A1), let us use the index  $i = l$  and  $j = l$  for the lowest levels of filled and empty clusters, respectively. Again, depending on the parent clusters, the lowest levels are at different energy separation from nearest neighbouring cluster. Thus we introduce two more subscripts,  $s_f$  and  $s_e$  respectively, for filled and empty clusters in unperturbed and perturbed eigen-values in Eq. (A1) as

$$|\Delta|^2 = \prod_{i=1}^M \prod_{j=M+1}^N \left[ 1 - \frac{2\delta_{i,s_f}^2}{(\epsilon_{j,s_e} - \epsilon_{i,s_f})^2} + \frac{\delta_{i,s_f} \delta_{j,s_e}}{(\epsilon_{j,s_e} - \epsilon_{i,s_f})^2} \right]. \quad (\text{A2})$$

Here  $\delta_{i,s_f} = \epsilon_{i,s_f} - \lambda_{i,s_f} = \delta$  for  $i \neq l$  and  $\delta_{i=l,s_f} = p D_{s_f-1}$ . Similarly,  $\delta_{j,s_e} = \epsilon_{j,s_e} - \lambda_{j,s_e} = \delta$  for  $i \neq l$  and  $\delta_{j=l,s_e} = p D_{s_e-1}$ . The clusterwise contributions to the

many-body overlap in Eq. (A2) can be written as

$$\log |\Delta|^2 = (T_0 + T_1 + T_2 + \dots). \quad (\text{A3})$$

$$\text{Here } T_0 = -\frac{\delta^2}{\omega_c^2} \sum_{j \in s_M} \sum_{\substack{i \in s_M \\ i \neq j}} \frac{1}{(\epsilon_{j,s_M} - \epsilon_{i,s_M})^2} \\ - p D_{s_M-1} (2p D_{s_M-1} - \delta) \sum_{j \in s_M} \frac{1}{(\epsilon_{j,s_M} - \epsilon_{l,s_M})^2}, \quad (\text{A4})$$

$$\text{with } \epsilon_{l,s_M} = \left( \frac{(s_M - 1)s_M}{2} + 1 \right) \omega_c.$$

$$T_1 = T_{1L} + T_{1U} + T_{LU}, \quad (\text{A5})$$

$$\text{with } T_{1L} = -\delta^2 \sum_{j \in s_M} \sum_{\substack{i \in s_{M-1} \\ i \neq j}} \frac{1}{(\epsilon_{j,s_M} - \epsilon_{i,s_{M-1}})^2} \\ - p D_{s_M-2} (2p D_{s_M-2} - \delta) \sum_{j \in s_M} \frac{1}{(\epsilon_{j,s_M} - \epsilon_{l,s_{M-1}})^2}, \quad (\text{A6})$$

$$\text{with } \epsilon_{l,s_{M-1}} = \left( \frac{(s_M - 2)(s_M - 1)}{2} + 1 \right) \omega_c$$

$$T_{1U} = -\delta^2 \sum_{\substack{j \in s_{M+1} \\ j \neq l}} \sum_{\substack{i \in s_M \\ i \neq l}} \frac{1}{(\epsilon_{j,s_{M+1}} - \epsilon_{i,s_M})^2} \\ - p D_{s_M-1} (2p D_{s_M-1} - \delta) \sum_{\substack{j \in s_{M+1} \\ j \neq l}} \frac{1}{(\epsilon_{j,s_{M+1}} - \epsilon_{l,s_M})^2} \\ - (2\delta^2 - \delta p D_{s_M}) \sum_{\substack{i \in s_M \\ i \neq l}} \frac{1}{(\epsilon_{l,s_{M+1}} - \epsilon_{i,s_M})^2} \\ - \frac{p^2 (2D_{s_M-1}^2 - D_{s_M}^2)}{(\epsilon_{l,s_{M+1}} - \epsilon_{l,s_M})^2} \quad (\text{A7})$$

$$\text{with } \epsilon_{l,s_{M+1}} = \left( \frac{s_M(s_M + 1)}{2} + 1 \right) \omega_c$$

$$T_{LU} = -\delta^2 \sum_{\substack{j \in s_{M+1} \\ j \neq l}} \sum_{\substack{i \in s_{M-1} \\ i \neq l}} \frac{1}{(\epsilon_{j,s_{M+1}} - \epsilon_{i,s_{M-1}})^2} \\ - p D_{s_M-2} (2p D_{s_M-2} - \delta) \sum_{\substack{j \in s_{M+1} \\ j \neq l}} \frac{1}{(\epsilon_{j,s_{M+1}} - \epsilon_{l,s_{M-1}})^2} \\ - (2\delta^2 - \delta p D_{s_M}) \sum_{\substack{i \in s_{M-1} \\ i \neq l}} \frac{1}{(\epsilon_{l,s_{M+1}} - \epsilon_{i,s_{M-1}})^2} \\ - \frac{p^2 (2D_{s_M-2}^2 - D_{s_M}^2)}{(\epsilon_{l,s_{M+1}} - \epsilon_{l,s_{M-1}})^2} \quad (\text{A8})$$

Here  $T_0$  represents the overlap from the main contributing cluster, *i.e.* the Fermi cluster. The next major contribution,  $T_1$ , comes from the neighbouring filled ( $s_{M-1}$ )

and empty ( $s_{M+1}$ ) clusters. Similarly,  $T_2$  represents contributions from next nearest neighbour filled ( $s_{M-2}$ ) and empty ( $s_{M+2}$ ) clusters and so on. Upon application of an attractive perturbation levels get shifted downwards. The amount of shift increases with increasing strength of perturbation. Thus for very weak perturbation, only the partially filled cluster participate in the many-body overlap, *i.e.*, Eq. (A3) reduces to calculating the first term in  $T_0$ . As known for systems with equi-spaced energy levels, the many-body overlap becomes  $|\Delta|^2 \sim (s_M)^{-\delta^2/\omega_c^2}$ , where  $s_M$  is the size of the last partially filled cluster. Now for a half-filled PQD with half-filled last cluster,  $s_M = \sqrt{N}$ . Thus for such a PQD subjected to *very weak perturbation*, the many-body overlap is given by

$$|\Delta|^2 \sim N^{-\frac{\delta^2}{2\omega_c^2}}. \quad (\text{A9})$$

The phase shift as quoted in the main text is  $\phi/\pi = \phi_c$  for core levels. For very large perturbations, all levels from different shells are at comparable distances (in energy space). In such a case, one can define a mean level spacing for the whole system as  $d = (s_n - 1)\hbar \left( \sqrt{(\omega_0^2 + \omega_c^2/4)} + \omega_c \right) / N \sim \sqrt{2/N} \hbar \omega_0$ . In this regime, many-body overlap of PQD with more or less equi-spaced levels is given by  $|\Delta|^2 \sim N^{-\delta^2/d^2}$ . In the intermediate regime of perturbation's strength one can not avoid neighbouring empty and filled shells of the last (partially) filled shell ( $s_M$ ). In this case Eq. (A3) reduces to  $\log |\Delta|^2 \sim T_0 + T_1$ . In the limit of a large cluster ( $s_M \gg 1$ ) and in the quasi-degenerate limit ( $\omega_0 \gg \omega_c$ ), Eq. (A) yields the many-body overlap as a function of cluster size ( $s_M$ ) as

$$|\Delta|^2 \sim (s_M)^{-\frac{\delta^2}{\omega_c^2}} \exp\left(-\frac{3}{2} p^2 s_M\right). \quad (\text{A10})$$

Note that  $0 < p < 1$  and  $p$  approaches 1 with increasing perturbation strength. For a half-filled PQD with half-filled last cluster under the *intermediate regime of perturbation* the many-body overlap as a function of  $N$  thus becomes

$$|\Delta|^2 \simeq N^{-\frac{\delta^2}{2\omega_c^2}} \exp\left(-\frac{3}{2} p^2 \sqrt{N}\right). \quad (\text{A11})$$

It would be worthy to mention that in Eq. (A10), there are two more exponentially decaying functions of  $s_M^2$  and  $s_M^3$  as  $\exp(-a s_M^2)$  and  $\exp(-b s_M^3)$  but the multiplicative factor  $a, b$  in the argument being very small, their contributions are negligible.

## ACKNOWLEDGMENTS

We thank H. Baranger, E. Mucciolo, G. Röder, J. Siewert, S. Tomsovic and D. Ullmo for several helpful discussions. S.B. thanks D. Chaudhuri for many useful discussions, and MPIPKS, Dresden for financial support, where a major portion of this work was done. M.H.

thanks the German Research Foundation (DFG) for support through the Emmy-Noether Programme.

- 
- [1] P. W. Anderson, *Phys. Rev. Lett.* **18**, 1049 (1967).
- [2] A. C. Hewson, *The Kondo Problem to Heavy Fermions*, Cambridge University Press, Cambridge, UK (1993).
- [3] G. D. Mahan, *Many Particle Physics*, 3rd ed., Kluwer Academic, Dordrecht, and Plenum Publishers, New York, 2000.
- [4] B. Roulet, J. Gavoret, and P. Nozières, *Phys. Rev.* **178**, 1072 (1969); P. Nozières, J. Gavoret, and B. Roulet, *Phys. Rev.* **178**, 1084 (1969); P. Nozières, and C. T. De Dominicis, *Phys. Rev.* **178**, 1097 (1969).
- [5] Y. Tanabe, and K. Ohtaka, *Rev. Mod. Phys.* **62**, 929 (1990) and references therein.
- [6] Y. Chen, and J. Kroha, *Phys. Rev. B*, **46**, 1332 (1992).
- [7] M. Reed, *Sci. Am.*, **268**, 118 (1993); M. A. Kastner, *Phys. Today*, **46**, 24 (1993); R. C. Ashoori, *Nature*, **379**, 413 (1996); L. P. Kouwenhoven, and C. M. Marcus, *Physics World* **11**, (1998).
- [8] L. L. Sohn, G. Schön, and L. P. Kouwenhoven, *Mesoscopic Electron Transport*, Kluwer, Dordrecht, 1997.
- [9] T. Blomquist, H. Schanze, I. V. Zozoulenko, H.-J. Stöckmann, *Phys. Rev. E* **66**, 026217 (2002).
- [10] C. M. Marcus, A. J. Rimberg, R. M. Westervelt, P. F. Hofkins, A. C. Gossard, *Phys. Rev. Lett.* **69**, 506 (1992).
- [11] R. O. Vallejos, C. H. Lewenkopf, and Y. Gefen, *Phys. Rev. B* **65**, 085309 (2002).
- [12] Y. Gefen, R. Berkovits, I. V. Lerner, and B. L. Altshuler, *Phys. Rev. B* **65**, 081106R (2002).
- [13] M. Hentschel, D. Ullmo, and H. U. Baranger, *Phys. Rev. Lett.* **93**, 176807 (2004).
- [14] Martina Hentschel, Denis Ulmo, and Harold U. Baranger, *Phys. Rev. B*, **72**, 035310 (2005).
- [15] Martina Hentschel, Denis Ulmo, and Harold U. Baranger, *Phys. Rev. B*, **76**, 245419 (2007).
- [16] L. P. Kouwenhoven, D. G. Austing and S. Tarucha, *Rep. Prog. Phys.* **64**, 701 (2001); L. P. Kouwenhoven *et al.*, *Science* **278**, 1788 (1997).
- [17] K. Ohtaka and Y. Tanabe, *Phys. Rev. B* **28**, 6833 (1983); Y. Tanabe and K. Ohtaka, *Phys. Rev. B* **29**, 1653 (1984).
- [22] For a comprehensive experimental review on the metallic case, see P. H. Citrin, G. K. Wertheim, and M. Schlüter, *Phys. Rev. B* **20**, 3067 (1979).
- [23] J. S. Lee, Y. Iwasa, and N. Miura, *Semicond. Sci. Technol.* **2**, 675 (1987); M. S. Skolnick, J. M. Rorison, K. J. Nash, D. J. Mowbray, P. R. Tapster, S. J. Bass, and A. D. Pitt, *Phys. Rev. Lett.* **58**, 2130 (1987).
- [24] S. Tarucha *et al.*, *Phys. Rev. Lett* **77**, 3613 (1996).
- [25] I. L. Aleiner and K. A. Matveev, *Phys. Rev. Lett.* **80**, 814 (1998).
- [22] For a comprehensive experimental review on the metallic case, see P. H. Citrin, G. K. Wertheim, and M. Schlüter, *Phys. Rev. B* **20**, 3067 (1979).
- [23] J. S. Lee, Y. Iwasa, and N. Miura, *Semicond. Sci. Technol.* **2**, 675 (1987); M. S. Skolnick, J. M. Rorison, K. J. Nash, D. J. Mowbray, P. R. Tapster, S. J. Bass, and A. D. Pitt, *Phys. Rev. Lett.* **58**, 2130 (1987).
- [24] S. Tarucha *et al.*, *Phys. Rev. Lett* **77**, 3613 (1996).
- [25] I. L. Aleiner and K. A. Matveev, *Phys. Rev. Lett.* **80**, 814 (1998).
- [26] G. Röder and M. Hentschel, in preparation.
- [27] The phase shift alone determines the many-body response in the x-ray edge problem. For example, in the photoabsorption case, an additional term, linear in the phase shift, appears.